

1    **A procedure for operational use of wave hindcasts to identify**  
2                                   **landfall of heavy swell**

3    Valdir Innocentini<sup>1</sup>, Ernesto Caetano<sup>2</sup> and Jonas Takeo Carvalho<sup>3</sup>

4           <sup>1</sup>Instituto Nacional de Pesquisas Espaciais, São José dos Campos, Brazil

5           <sup>2</sup>Institute of Geography, National Autonomous University of Mexico, Mexico

6           <sup>3</sup>Rede de Modelagem e Observação Oceanográfica, Centro de Hidrografia da  
7                                   Marinha, Niterói, Brazil

8                                   *Corresponding author adress:*

9                   Dr. Valdir Innocentini, INPE, Av. dos Astronautas, 1756,

10                                   São José dos Campos - SP

11   Brazil

12                                   E-mail: valdir@cptec.inpe.br

13   (June 2013)

## Abstract

The wave pattern on the Brazilian coastline is composed of both wind waves and swell. The wave systems (WSs), extracted from the spectra near the coast produced by numerical wave models, reveal the occasional presence of intense swells, with small significant wave height ( $H_S$ ) and large average period ( $T_a$ ). This kind of event has nearly no effect over deep water, but its landfall can be accompanied by inundation, mainly when coupled with favourable tides and storm surge. Since these events are not clearly evident in the bulk parameters, this study proposes a methodology to i) identify intense swells simulated by a coarse grid resolution wave modelling system (CWS), and to ii) evaluate their importance.

In this methodology, monitoring sites are defined along a 100-m isobath contouring the Brazilian coast, where the CWS hindcasts the spectra for a 31-year period, from 1979-2009, obtained by the WAVEWATCH wave model. The spectra are partitioned into WSs, which are used to build cumulative distribution tables (CDT) for each site. The variable used in the CDT is the flux of energy per unit length perpendicular to the wave propagation ( $P_W$ ), which contains in its definition both  $H_S$  and  $T_a$ . The direction of propagation of a WS is used to compute the components of  $P_W$  parallel and perpendicular to the coast. From the CDT of the perpendicular component of  $P_W$ , the percentile of an incoming WS can be found and its intensity ranked.

To illustrate the feasibility of this proposal, the method is used to find the

38 50 most powerful distantly-generated swells for two sites, one on the north-  
39 ern and another on the southern Brazilian coast. In addition, the method is  
40 applied in two case studies, both accompanied by coastal flooding and ero-  
41 sion: one represents a very powerful WS arriving at the northern coast and  
42 the another a less energetic event occurring on the southeastern coast. The  
43 analysis of bulk parameters fails to identify the second case as potentially  
44 destructive, while the proposed methodology clearly gives some indication.

## 45 **1. Introduction**

46 In operational numerical weather prediction, accurate forecasting of some events  
47 demands high spatial and temporal resolution, which may be a major impediment  
48 due to high-performance computer resource requirements. A less computer in-  
49 tensive approach is to run a lower resolution model and to monitor the precursors  
50 of the target event. When certain specific conditions are satisfied a high resolu-  
51 tion and accurate numerical simulation is carried out. As examples the predictive  
52 scheme for the Atlantic basin tropical cyclones, using West African rainfall as  
53 predictor (Gray and Landsea 1992), and for tornado development, where a set of  
54 observational and numerically simulated precursors is monitored (Paice 1998).

55 A similar situation is found in oceanic wave prediction near the coastline. Usu-  
56 ally a coarse grid global wave modeling system (CWS) simulates the generation  
57 and propagation of the wave spectra over deep water up to the 100-m isobath fol-  
58 lowing the coast. However, for accurate prediction in shallow water and areas near  
59 the coastline, a fine grid wave modeling system (FWS) with a very high bathymet-  
60 ric resolution and appropriate representation of physical processes is applied.

61 The ideal configuration should incorporate the FWS in a coastal modeling  
62 system able to combine tides, surges, waves and wave-current interaction, such as  
63 that used by Brown and Wolf (2009) in a case study of surge occurring in north-  
64 western England. Unfortunately, in many forecasting centers, only the CWS is  
65 operationally available, and when a powerful fetch (large area with homogeneous  
66 surface wind blowing for several hours) develops near the coast and the wave

67 model presents significant wave height ( $H_S$ ) greater than about 2.5 m propagating  
68 toward the coast, the forecaster issues an warning. In general the forecast analysis  
69 is based on bulk parameters such as  $H_S$ , average period ( $T_a$ ), peak period ( $T_p$ ),  
70 and their respective directions, all computed from the energy spectrum, which is  
71 the wave model prognostic variable.

72 In countries with an extensive coastline, e.g. Brazil with more than 9000 km, it  
73 is impossible to maintain an operational coastal modeling system . A realistic and  
74 sound alternative is to develop a set of tools producing predictors and to leave the  
75 coastal system (composed of several numerical models) in stand-by mode, waiting  
76 to be activated for a critical region when necessary . However the bulk parameters,  
77 in the case of the Brazilian coast, are not sufficient either for the forecast analysis  
78 nor as a predictor for the FWS due to the complexity of incident wave systems.  
79 More suitable parameters must be extracted from the spectra.

80 The Brazilian coast spans latitudes 34°S to 3°N , and has a geographic config-  
81 uration exposing it to waves generated by wind regimes within semi-permanent  
82 and migratory meteorological phenomena. The northern and northeastern coast-  
83 lines receive the gentle nearly unchanging waves generated by the widespread  
84 fetch within the trade winds, while the semipermanent anticyclone positioned  
85 over the South Atlantic forms northeasterly waves incident on the northeastern  
86 and southeastern coast. On the other hand, migratory extratropical cyclones, in  
87 both hemispheres, generate waves incident on almost all the Brazil's coastline,  
88 except perhaps the northern part of the northeastern coast from 10°S to 5°S. The  
89 coastline facing the North Atlantic receives swell generated by distant extratropi-

90 cal cyclones during the North Hemisphere winter causing some damage (Innocen-  
91 tini et al. 1999). However, the most extreme waves are imposed by extratropical  
92 cyclones developing over the South Atlantic, so they have received more attention  
93 from researchers (e.g. Innocentini and Caetano Neto 1996; Rocha et al. 2000).

94       Regarding extreme events, some researchers emphasize the location of the  
95 associated extratropical cyclone. Two regions in the South Atlantic are highlighted  
96 by Sinclair (1995) as cyclogenetic, east of Argentina (45°S) and east of Uruguay  
97 (30°S). Rocha et al. (2004) studied six extratropical cyclones in 1999 developing  
98 in these two regions with the NCEP-NCAR reanalysis (Kalnay et al. 1996). The  
99 mature stage (stronger surface winds) were localized within 35°- 30°S and 45°-  
100 30°W, with east, southeast and northward trajectories. Machado et al. (2010)  
101 selected 40 extreme events with  $H_S > 6$  m, very close to the south Brazilian  
102 coast, from the wave hindcast obtained using the WAVEWATCH model for the  
103 period 1979-2009: 80% of the cases are developed over the ocean just offshore of  
104 Uruguay.

105       Since these studies concern extreme  $H_S$  occurrences west of 30°W (not too  
106 far from the coast), the analysis of the bulk parameters is sufficient to carry out  
107 the investigation because only one wave system plays the main role in forming the  
108 wave pattern relevant to the coast.

109       However, a closer examination of the spectra along the southern and south-  
110 eastern Brazilian coastline reveals that it is common to have two or three wave  
111 systems, one due to local wind (wind sea) and others propagating from distant  
112 regions, outside those contemplated by the cited studies.

113 For a fixed observer, the further away a wave system has been generated, the  
114 smaller the  $H_S$  and the larger the  $T_p$ . However, it may contain energy large enough  
115 so that  $H_S$  becomes very high when the waves are traveling over shallow water, as  
116 in a *meteorological tsunami*, but the standard analysis based on bulk parameters  
117 would hardly detect its importance. As it will be shown, a wave system with  $H_S =$   
118 4 m and  $T_a = 6$  s has smaller wave power than a wave system with  $H_S = 2.5$   
119 m and  $T_a = 16$  s: both cases represent favorable scenarios for damage along the  
120 coast, but in the second case (generated from east of longitude  $30^\circ\text{W}$ ) this is not  
121 revealed by the bulk parameters.

122 The main objectives of this study are i) to present a procedure to identify  
123 energetic swells simulated by a CWS propagating from a distant storm, and ii) to  
124 find cases of distantly generated strong swell reaching the Brazilian coast and to  
125 identify the associated meteorological events.

126 Here, the spectrum is partitioned into wave systems, which are evaluated by  
127 their wave power or energy flux. First of all, it is necessary to know the clima-  
128 tology of the wave systems incident on the Brazilian coast. This will be carried  
129 out in three steps: i) hindcast a database composed of spectra every 3 hours at  
130 61 virtual sites along the 100-m isobath; ii) extract the wave systems from each  
131 spectrum, computing their properties; iii) generate percentile tables for the flux of  
132 energy. These procedures are discussed in Section 2. Section 3 presents the main  
133 features of the stronger events generated in the North Atlantic (South Atlantic)  
134 arriving at the northern (southeastern) Brazilian coast with  $T_p > 15$  s. Section 4  
135 applies the methodology to two case studies, and finally Section 5 summarizes the

136 main results. The present paper, designated as part I, presents the basic methodol-  
137 ogy in order to illustrate its potential. In another study, part II, observations near  
138 the coast and a FWS will be used to assess the accuracy of this methodology in  
139 providing the predictors.



## 140 **2. Description of the procedure**

141 An operational scheme for numerical wave prediction can be composed of two  
142 systems of grids: a set of coarse resolution grids (CWS), where the waves are  
143 accurately simulated over deep ocean and the wind forcing is essential, and a set  
144 of finer grids (FWS), where the coastline and bathymetry are accurately repre-  
145 sented in order to modify the waves propagating towards the coast with shallow  
146 water wave physics incorporated. Usually the grid resolutions are  $0.1 - 1^\circ$  (CWS)  
147 and 50-2000 m (FWS). The 100-m isobath is a reasonable reference depth for  
148 separating the two grid systems.

149 Since the CWS deals with global or very large domains, the WAVEWATCH  
150 III model (Tolman 2008, hereafter WW3) is used to simulate the spectral wave  
151 energy generated by the surface wind. Simulations in coastal water are required  
152 from the FWS and the SWAN model (Booij et al. 1999) provides an appropriate  
153 solution, one that has been used in many studies (e.g. Brown and Wolf 2009).

154 The approach adopted in this study consists of identifying signatures or key  
155 factors in energetic events simulated by the CWS having potential to cause dam-  
156 age to the coast. In conjunction with other predictors (e.g. tides and coastal cur-  
157 rents) the forecasters can make decisions, as for example to trigger the FWS. The  
158 development of a tool able to evaluate the strength of an event is based on three  
159 steps: i) a long period hindcast and the definition of a set of monitoring sites  
160 along the 100-m depth isobath following the Brazilian coastline; ii) the partition  
161 of the spectra at each monitored site into WSs; iii) construction of tables with the

162 cumulative distribution of variables computed from the WS.

163

164 *a. The hindcast wave spectra and sites*

165 Saha et al. (2010) developed a new coupled global NCEP Climate Forecast  
166 System Reanalysis (CFSR) for the period 1979-2009. The database includes ice  
167 surface coverage and 10-m winds with spatial and temporal resolutions of  $0.3125^\circ$   
168  $\times 0.3125^\circ$  and 1 h, respectively. The CFSR provides a wind forcing for wave mod-  
169 els with a resolution higher than any previous available reanalysis. The wave hind-  
170 cast is generated by the WW3 using a global domain and three nested domains,  
171 forced by the surface winds produced by the CFSR analysis for the 1979-2009 pe-  
172 riod. The global resolution is  $0.625^\circ \times 0.625^\circ$  and the three nested domains cover  
173 all of the Brazilian coast (Fig.1), with resolution  $0.3125^\circ \times 0.3125^\circ$ . The output  
174 produced by the WW3 simulations consists of average parameters extracted from  
175 the spectrum at all grid points and the spectra at 61 monitoring points along the  
176 100-m isobath line following the Brazilian coast (Fig. 1) at 3-h intervals. The  
177 spectral database constitutes the main source for evaluating the strength of incom-  
178 ing wave systems with potential for causing damage to the coastline.

179

180 *b. Wave system and potential significant height*

181 Usually a spectrum is composed of several clusters or WSs, generated by dif-  
182 ferent meteorological events. Many times a WS travels several thousand kilome-  
183 ters before reaching the coastline. There are a number of algorithms for parti-  
184 tioning the spectrum into WSs (Gerling 1992; Hasselmann et al. 1994; Hanson

185 and Phillips 2001). A comparison among some of these schemes is presented by  
186 Portilla et al. (2009).

187 The partition of the spectrum used in this research is performed in three steps:  
188 i) identification of maxima; ii) association of spectral elements with a maximum  
189 and; iii) merging groups. A spectral element is a maximum when all surround-  
190 ing elements are smaller: since the spectrum is discretized into directions and  
191 frequencies, each spectral element is surrounded by 8 elements, except those with  
192 minimum or maximum frequency which are surrounded by only 5 elements. Each  
193 maximum defines the first element of a WS, and a label is attributed to each one  
194 (e.g., 1, 2, 3, etc ...). The next step is to find the parent of each spectral element,  
195 defined as the element among its neighbors whose spectral energy is greatest; each  
196 spectral element is assigned the same label as the parent. We found that four scans  
197 (across the frequencies and directions) in searching for the parent of each element  
198 are enough to label all elements. Finally, when a WS has a very small energy con-  
199 tent it is discarded, and if two WSs are too close they are merged following the  
200 criteria suggested by Hanson and Phillips (2001). The main differences among  
201 the methods are the merging criteria, but at this moment this is not crucial to this  
202 study.

203 For each WS the usual parameters are computed: significant wave height  $H_S$ ,  
204 average period  $T_a$ , peak period  $T_p$ , and their respective directions. However, in  
205 order to access the energy content of a WS, the wave power  $P_W$ , defined here as  
206 the flux of energy per unit length perpendicular to the wave propagation (the rate  
207 which the wave energy is advected - see Young, 1999, page 16), is also calculated.

208 It is given by

$$209 \quad P_W = \rho g \int_0^\infty c_g(f)E(f)df$$

210 where  $c_g(f)$  is the group velocity,  $\rho$  the density,  $g$  the gravitational acceleration,  
211  $f(\equiv 1/T)$  the frequency,  $T$  the period, and  $E(f)$  the unidimensional frequency  
212 variance density spectrum. Defining the average group velocity by

$$213 \quad \bar{c}_g \equiv (1/\bar{E}) \int_0^\infty c_g(f)E(f)df$$

214 where

$$215 \quad \bar{E} = \int_0^\infty E(f)df$$

216 it follows that

$$217 \quad P_W = \rho g \bar{c}_g (H_S/4)^2$$

218 where  $H_S \equiv 4\sqrt{\bar{E}}$ . For deep water,  $c_g = g/(4\pi f) = gT/(4\pi)$ , then

$$219 \quad P_W = \frac{\rho g^2}{64\pi} H_S^2 T_a$$

220 A similar formulation can be found in many texts, as for example Dean and Dal-  
221 rymple (2003). Often  $P_W$  is expressed in the international system of units (e.g.  
222 Sasaki 2012):

$$223 \quad P_W \approx 0.5 H_S^2 T_a \quad [\text{kW/m, m, s}]$$

224 where  $H_S$  and  $T_a$  must be expressed in meters and seconds, respectively. It must  
225 be emphasized that this relationship is true only in deep water.

226 For a convenient interpretation of the results, the potential significant height  
227  $H_{SP}$  replaces the wave power. It is defined as the  $H_S$  which the WS would have  
228 if its period were 10 s. Then for a WS with wave power  $P_W$ ,  $H_{SP}$  is given by

$$229 \quad H_{SP} = \sqrt{\frac{P_W}{10 \times 0.5}} \quad [\text{m}]$$

230 One needs to keep in mind that  $H_{SP}$  is just a form to express the wave power, and  
231 its value never can be compared with  $H_S$ . Therefore the choice of 10 s is arbitrary  
232 and any other value could be chosen, without any detriment to the discussion.

233

234 *c. The cumulative distribution of potential significant height*

235 In order to classify the strength of a particular WS, the  $H_{SP}$  of all WSs re-  
236 ported at a site must be known. The information must be organized in a database,  
237 so that the statistical percentile of the target incoming event can be determined.  
238 For this purpose, the cumulative distribution tables (hereafter CDT) are constructed  
239 for the period 1979-2009 at each site along the 100-m isobath.

240 More specifically, four CDTs for  $H_{SP}$  are computed for each site: according  
241 to the peak direction of a WS,  $H_{SP}$  is decomposed into components perpendicular  
242 and parallel to the 100-m isobath. Depending on its direction, the  $H_{SP}$  parallel  
243 component can be from the right or left. Here the forward direction is taken in  
244 the sense of the motion vector of the WS towards the coast. Then each computed  
245 value is tabulated with 0.1 m class intervals, and the CDTs obtained are : i) total;  
246 ii) perpendicular; iii) from the left; and iv) from the right. Cases with  $H_{SP} < 0.5\text{m}$

247 are excluded.

248 Note that for the WS we are using  $T_a$  to compute  $P_W$ , but the decomposition  
249 is done with  $T_p$ . Although quite distinct for the entire spectrum, they are very  
250 similar for a simple WS.

### 251 **3. The generating region and characteristics of some** 252 **cases**

253 The incident  $H_{SP}$  decomposed into directions parallel and perpendicular to the  
254 100-m isobath according to their peak frequency direction are denoted by  $H_{SP}^{par}$   
255 and  $H_{SP}^{per}$ , respectively. The main focus is on the perpendicular component, which  
256 in principle has more potential to penetrate and affect the coastline. In this section  
257 the main properties and trajectories of the meteorological events responsible for  
258 the generation of WS incident on the north and south Brazilian coast with small  
259  $H_S$  and high  $H_{SP}^{per}$  will be described.

260

#### 261 *a. The percentile along the coast*

262 Fig. 2 shows the percentile of  $H_{SP}^{per}$  for the 61 sites for the period 1979-2009,  
263 following the procedure outlined in Section 2. The coastline from point 1 to 7  
264 receives the most energetic events, 0.1 % of the cases having  $H_{SP}^{per} > 5$  m. From  
265 site 8 almost to site 38, the  $H_{SP}^{per}$  with percentile 0.1 % decreases, and from site 39  
266 on there is a small tendency towards having more energetic events. Some excep-  
267 tions to these general tendencies must be mentioned, as for example around site  
268 25, where the continental shelf extends towards the ocean (Abrolhos Banks). Sites  
269 38 and 45 demarcate the boundary between two different wave climate regimes  
270 where WSs are more energetic - more southern sites are associated with the prox-  
271 imity of cyclogenesis regions of the South Atlantic, meanwhile the reason for  
272 most energetic events toward the north is not immediately evident and research is

273 required (this is beyond the scope of this paper).

274

275 *b. The 50 most intense events for sites 22 and 47*

276 The evolution of a WS generated near a site is characterized by an initially  
277 small  $T_p$  increasing as the WS becomes more energetic. In contrast, a distantly  
278 generated WS is identified first by a high  $T_p$ , which decreases slowly as the energy  
279 associated with smaller periods arrives. As a general rule, the further away the WS  
280 has been generated the slower the decrease of  $T_p$ , and for a distantly generated WS  
281  $T_p$  remains nearly constant. Since the main interest here concerns cases that are  
282 distantly generated, the highest  $H_{SP}^{per}$  with  $T_p \geq 15$ s will be selected. Only cases  
283 at sites 22 and 47 will be presented, since their locations seem to be representative  
284 of incident swells from the South and North Atlantic, respectively.

285 Often the arrival of a WS with  $T_p \geq 15$  s is observed at a certain time, but does  
286 not maintain this characteristic over the next 3 h, that is,  $T_p < 15$  s. This means  
287 the WS was not generated so far away or else it merged with another WS. For this  
288 reason, a WS will be selected only when  $T_p$  remains smaller than 15 s for a time  
289 period equal or greater than 9 h.

290 Fig. 3 shows  $H_{SP}^{per}$ ,  $H_S$ , and  $H_{SP}$  for the strongest  $H_{SP}^{per}$  events for both sites.  
291 At site 22, in general,  $H_S$  and  $H_{SP}$  are much larger than the respective  $H_{SP}^{per}$ ,  
292 whereas at site 47  $H_S$  is smaller and  $H_{SP}$  greater than  $H_{SP}^{per}$ . This means that  
293 the perpendicular wave power is better configured for 47, because for site 22 a  
294 large quantity of parallel energy flux is present. This is an expected result since  
295 the parallel energy at 47 is mainly due to the trade winds, which are persistent



296 but not as strong as the winds in the South Atlantic for an extratropical cyclone  
297 developing near the coast, thus site 22 receives a substantial amount of parallel  
298 energy from the south.

299 Comparing the two sites,  $H_{SP}^{per}$  is larger for 47, which is due to its privileged  
300 location in receiving perpendicular energy from distantly generated WS coming  
301 from the North Atlantic.

302

### 303 *c. The trajectories of some events*

304 A detailed examination of the WSs presented in Fig. 3a revealed some with  
305 high  $H_S$  generated west of longitude  $30^\circ\text{W}$ , e.g. cases 5, 6, 8, etc. Certainly,  
306 they could be very easily detected by the bulk parameters. There were also other  
307 cases generated very far from site 22, but they merged during the propagation  
308 with nearby generated WS losing the characteristics of a distantly generated swell.  
309 However, from the detailed examination, cases were obtained with percentile of  
310  $H_S$  greater than 20%, corresponding to  $H_S \leq 1.8$  m for site 22, generated east-  
311 ward of longitude  $30^\circ\text{W}$  and reaching the site without having been contaminated  
312 by nearby generated WS. Inspection of Fig. 3a reveals 15 cases satisfying this  
313 condition, whose main properties are listed at Table 1.

314 The location of site 22 is more likely to receive higher  $H_{SP}^{per}$  from meteo-  
315 rological events developing further north over the Atlantic. During the months  
316 November, December and January no WS is reported in Table 1, because during  
317 this period the energetic meteorological events developed at higher latitudes.

318 The trajectories of these 15 cases were tracked through the region where the

319 winds were greater than 20 m/s, and the position of the centre of the area with  
320 stronger winds is depicted in Fig. 4. Each trajectory is labeled with the event  
321 number indicated in Table 1. Most of the cases have their entire trajectory east-  
322 ward of 30°W, except events 41 and 43. The most distant event is 29, occurring  
323 on June 2007.

324 A quite distinct situation is observed at site 47, because all events selected are  
325 distantly generated, without the necessity of the imposition of an additional filter  
326 for  $H_S$ . Table 2 presents the main features of the 10 strongest WSs shown in Fig.  
327 3b, and their trajectories in Fig. 5. From Fig. 3b, events 1 and 2 were the most  
328 powerfull not only for  $H_{SP}^{per}$ , but also for  $H_S$ . The trajectory of the associated  
329 fetch revealed both translating northwards. The final stages of the trajectories in  
330 Fig. 5 were reported eastward of longitude 50°W. The trajectories westward of  
331 this longitude are associated with smaller  $H_{SP}^{per}$ . For example, events 37 and 48 in  
332 Fig. 3b presented very high  $H_S$ , but small  $H_{SP}^{per}$ , and a closer examination in both  
333 cases revealed that their most energetic phase was westward of longitude 50°W  
334 (not shown).

## 335 **4. The method applied to two illustrative cases**

336 As outlined in the previous section, the analysis based on percentiles of WSs is a  
337 useful tool to identify and evaluate events with low  $H_S$ , but high  $T_p$  so the wave  
338 power is high. In particular the component  $H_{SP}^{per}$  was emphasized, since it rep-  
339 resents the energy that can cross the shallow bathymetry and reach the coastline.  
340 Thus the objective here is focused on the wave power of a WS, which is often  
341 ignored in the evaluation of wave events.

342 In this section a set of procedures is described and applied to two special cases,  
343 one reaching the northern and other the southern Brazilian coastline. Both cases  
344 represent waves distantly generated by extratropical cyclones. Although there  
345 are no observational data available to confirm their importance, both cases were  
346 widely commented upon by the media. Briefly, they are:

- 347 • Case 28 March 2011: associated with erosion and inundation on the coast  
348 around site 22;
- 349 • Case 15 January 2013: responsible for the sinking of at least 5 boats on the  
350 northern Brazilian coast and inundation around site 47.

351 It is shown that the standard analysis based on bulk properties computed from  
352 the spectrum may fail in the identification of an energetic swell. An alternative  
353 approach, proposed to access the swell strength near the coastline, is applied in  
354 both cases. The strategy to evaluate the events is composed of these three steps: i)  
355 description of both spatial distribution and time evolution of bulk parameters at the

356 target site; ii) discussion of Hovmöller diagrams; iii) examination of development  
357 of WSs at the target site and identification of the strongest ones.

358

359 *a. The case of 28 March 2011*

360 The importance of this case resides mainly in the erosion damage with extensive  
361 inundation along the coastline near site 22 reported by the media.

362

363 1) GENERAL DESCRIPTION

364 At 2100 UTC 28 March 2011 a large area with  $U_{10} > 24 \text{ m s}^{-1}$  with direction  
365 towards the Brazilian coast was identified (Fig. 6). The distance of this fetch to  
366 site 22 was about 3,700 km. The fetch with  $U_{10} > 24 \text{ m s}^{-1}$  traveled through the  
367 area encompassed by latitudes  $45^\circ$  and  $35^\circ$  S, and longitudes  $10^\circ$  W and  $0^\circ$  during  
368 a 54-hour period, from 2100 UTC 27 to 0300 UTC 30 March 2011. Afterwards,  
369 the wind speed decreased while the core moved eastward, stopping the process of  
370 intense wave growth. In the generating area  $H_S$  increased to more than 10 m at  
371 0600 UTC 29 March with average direction towards the Brazilian coast, as shown  
372 in Fig. 7 where the  $H_S$  contour and mean wave vector are depicted. Since the  
373 generating wave area was far away, only swell could be expected at site 22.

374 Fig. 8 presents the time evolution of  $T_p$  and  $H_S$  at site 22. As one can observe,  
375  $H_S$  presents a small rise late on 01 April, however the presence of swell is evi-  
376 denced by an abrupt jump of  $T_p$  to 15 s. Further insight can be obtained from the  
377 spectrum, represented in Fig. 9 at 1800 UTC 01 April. The spectrum is composed  
378 of at least 4 WSs, but the one propagating from the southeast with  $T_p = 15 \text{ s}$  was

379 responsible for the coast damage.

380 For decision makers any harmful consequence of this swell was not evident  
381 from the analysis of the standard parameters. The evolution of the swell, while  
382 propagating from the 100-m isobath towards the coast, is determined by the bathy-  
383 metric configuration and only a finer resolution wave model is able to realistically  
384 reproduce the swell modification over that region and its landfall impact. Thus,  
385 further information about the spectra is required to assess the importance of this  
386 event.

387

## 388 2) THE HOVMÖLLER DIAGRAM

389 An efficient method for assessing a general picture about the wave conditions  
390 along the coast is the use of the Hovmöller diagram for all variables. In particular,  
391 when applied to  $H_{SP}^{per}$  and its percentile, an interpretation is obtained that gives  
392 insight about the wave regarding the eventual propagation towards the coastline.  
393 As a first attempt a rough overview can be useful with this variable computed us-  
394 ing the average  $H_S^{per}$  and  $T_p$  from the full spectrum. In general, one can expect  
395 this procedure to result in  $H_{SP}^{per}$  greater than those from individual WS, but it will  
396 indicate if further analysis is necessary. Fig. 10 presents the Hovmöller diagram  
397 for these two variables produced by the WW3 for a forecast period extending to 5  
398 days - the vertical dashed line at 00 UTC 30 March separates the first day forecast  
399 from the previous period. The figure does not show high  $H_{SP}^{per}$  in locations around  
400 site 22, but the percentile became smaller than 6% late on 01 April, indicating that  
401 individual WSs deserve more careful and detailed examination.

402

### 403 3) THE EVOLUTION OF THE WS

404 Fig. 11 presents the evolution of  $H_{SP}^{per}$  for individual WSs at site 22 for a  
405 4-day period beginning 30 March. The horizontal line indicates the percentile  
406 of the maximum  $H_{SP}^{per}$  obtained. The partition at each time is carried out by the  
407 method presented in Section 2. Two WSs at consecutive times are connected if  
408 the direction and  $T_p$  differences are less than  $20^\circ$  and 10%, respectively.

409 By 1200 UTC 01 April a WS with  $H_{SP}^{per} = 0.9$  m struck site 22 and became  
410 strongest early on 02 April, with a percentile of 4.7%. However these results are  
411 not sufficient to explain the inundation reported at this site. Others properties that  
412 could play a relevant role in increasing the water level must be considered, namely  
413 wind, surface pressure, and tides. An inspection of the wind and surface pressure  
414 fields reveals that they were very weak around site 22 and unlikely to contribute to  
415 enhancing the water level (not shown). However, the tide was rising and near its  
416 maximum level of about 0.7 m on 01 April (not shown), therefore its constructive  
417 combination with the distantly generated swell seems to provide the additional  
418 ingredient for the inundation and erosion reported in the coastal area behind site  
419 22.

420

#### 421 *b. The case of 15 January 2013*

422 This case was reported by the media as very destructive, responsible for several  
423 kinds of damage along a large section of the coast around site 47. Despite the  
424 great distance between the wave generating area and this site (near 6000 km), the

425 winds were very strong, and thus powerful WSs hit the northern Brazilian coast  
426 with pronounced strength.

427

## 428 1) GENERAL DESCRIPTION

429 On 10 January 2013 an extratropical cyclone crossed the east coast of North  
430 America near  $43^{\circ}\text{N } 70^{\circ}\text{W}$ , and moved slowly eastwards while a prominent fetch  
431 with wind speeds higher than  $20 \text{ m s}^{-1}$  was spawned over a large area. During  
432 a 24-h period, from 00 UTC 11 January, the winds were higher than  $24 \text{ m s}^{-1}$   
433 blowing south-southeastward. Fig. 12 presents the wind fields at 1800 UTC 11  
434 January, with a large fetch on the left flank of the cyclonic circulation.

435 The cyclonic circulation remained anchored nearly at the center of the North  
436 Atlantic during its life-cycle, while the sea surface wave energy increased sub-  
437 stantially in response to such strong winds. The maximum  $H_S$  were higher than  
438 12 m at 0900 UTC 12 January (Fig. 13). Over the following days a large quantity  
439 of wave energy propagated towards the north Brazilian coast.

440 The time evolution of  $T_p$ ,  $H_S$ , and  $U_{10}$  at site 47 can be examined in Fig. 14.  
441 The abrupt jump of  $T_p$  early on 15 January shows the swell's arrival - note  $T_p > 15$   
442 s for a period of about 40 h. During nearly all of 16 January the persistence of  
443  $H_S > 3 \text{ m}$  indicates a very high flux of energy.

444 The spectral distribution of energy was at its maximum intensity at 0600 UTC  
445 16 January when  $H_S = 3.16 \text{ m}$  (Fig. 15). A weaker west-northwesterly WS with  
446  $T_p < 10 \text{ s}$  is due to the trades, while another stronger is propagating from the ex-  
447 tratropical cyclone located in the North Atlantic, with  $T_p > 15 \text{ s}$ . This description

448 is enough to conclude that this is a very powerful WS, however further detailed  
449 analysis is necessary to reveal its importance.

450

## 451 2) THE HOVMÖLLER DIAGRAM

452 The diagram represented in Fig. 16 shows a large  $H_{SP}^{per}$  striking site 60 late  
453 on 14 January. Since this site is further north, it is one of the first to receive the  
454 swell. During the next 48 hours  $H_{SP}^{per} > 2.5$  m spreads eastward along the north-  
455 ern Brazilian coast. The percentile  $< 1\%$  evidences the powerful nature of this  
456 event.

457

## 458 3) THE EVOLUTION OF THE WS

459 The evolution of the WSs composing the spectrum from 13 to 16 January  
460 2013, can be examined in Fig. 17. The stronger WS arrived at site 47 early on 15  
461 January, and  $H_{SP}^{per}$  increases during the next 24 hours. The peak value was 2.8 m  
462 at 0900 UTC 16 January, corresponding to a percentile  $< 0.1\%$ . Certainly, this  
463 description provides very reliable information for disseminating a warning.



## 464 **5. Summary and conclusions**

465 Several operational forecasting centers produce daily bulletins reporting sea sur-  
466 face waves and issue warnings in case of intense events over the open sea or  
467 of shoreline flooding based on the analysis of numerical simulations. For open  
468 sea, where the seafarers are the main interested parties, a standard procedure is  
469 adopted, which consists of monitoring the behavior of averaged (or bulk) param-  
470 eters computed from the simulated wave spectrum, e.g. significant wave height  
471 ( $H_S$ ), average period ( $T_a$ ), and peak period ( $T_p$ ). In shallow water near the coast  
472 a more complex procedure must be implemented, including tides, storm surge  
473 caused by wind and sea level pressure, coastal circulation, and near shore shallow  
474 water wave forecasting. Large computational power is necessary for an extensive  
475 coastline, because the appropriate models require high resolution grids.

476 To save computer time and to provide guidance for the warning service for  
477 shallow water, the search of precursors indicating a possible incidence of high  
478 waves on the coast is a useful tool. However the analysis of the bulk parameters  
479 does not reveal the potential increase of the waves while propagating over shallow  
480 water. A more suitable variable is the flux of energy, or wave power, defined in  
481 deep water as  $P_W = 0.5H_S^2T_a$ . Since it contains both  $H_S$  and  $T_a$ . Large  $T_a$  is  
482 the signature of an energetic swell, which can have increasing  $H_S$  as it propagates  
483 over shallow water. Also, the spectrum is formed by several wave systems (WS),  
484 some of which are propagating parallel to the coast and are less likely to reach the  
485 coast. Then, to evaluate  $P_W$  individually for each WS, selecting the most likely to

486 propagate towards the coast, gives a better way to search for precursors.

487 In this study, a methodology to evaluate the strength of a WS and its use as a  
488 precursor of coastal monitoring through the results of numerical forecasting ob-  
489 tained by the model WAVEWATCH is presented and is applied to the Brazilian  
490 coast.

491 Initially, a set of monitoring sites is defined, located on an isobath where the  
492 incident waves have suffered small influence of the seabed topography; for the  
493 Brazilian coastline 61 sites, about 100 km apart, were chosen on the 100-m bathy-  
494 metric depth contour. On these sites the spectra produced by WAVEWATCH are  
495 separated into WSs, and their properties are evaluated. In order to facilitate the  
496 interpretation, the wave power is replaced by a new variable, potential significant  
497 wave height ( $H_{SP}$ ), defined as the significant height for the same  $P_W$ , but with  
498  $T_a = 10$  s, i.e.,  $H_{SP} = [P_W / (0.5 \times 10)]^{0.5}$ . Additionally, according to the peak  
499 period direction of the WS,  $H_{SP}$  is decomposed into perpendicular ( $H_{SP}^{per}$ ) and  
500 parallel ( $H_{SP}^{par}$ ) directions relative to the 100-m isobaths orientation.

501 The spectra for the sites from 1979 to 2009, provided by WAVEWATCH  
502 forced by the surface wind fields from the global NCEP Climate Forecast Sys-  
503 tem Reanalysis (CFSR), were partitioned into WSs. Then, for each site, cumula-  
504 tive distribution tables (CDT) were constructed for the WSs, so any event can be  
505 ranked and its relative importance expressed by percentiles.

506 The methodology were applied with two objectives: i) to detect distantly gen-  
507 erated WS reaching the Brazilian coast within the 31-year period run, and ii) to  
508 evaluate the strength of incident WS in an operational service.

509 For the first objective, two sites with quite different locations were selected,  
510 one exposed to meteorological events developing over the Central and South At-  
511 lantic Ocean (site 22, at 22.09S-319.93E), the other developing over the North  
512 Atlantic Ocean (site 47, at 2.23S-320.04E). All WSs simulated by the long-period  
513 run, arriving at these two sites with  $T_p > 15$  s during a period of at least 9 hours,  
514 were selected and ordered by the value of  $H_{SP}$ ; the 50 strongest cases were ex-  
515 amined. For site 22 it was found that many cases were not distantly generated.  
516 However, when an additional filter was imposed in the form of percentile of sig-  
517 nificant wave height  $H_S$  greater than 20% (corresponding to  $H_S < 1.8$  m for this  
518 site), only distant cases remained: the associated fetches (defined as a large area  
519 with  $U_{10} > 20$  m s<sup>-1</sup>) arose south of 39°S and west of 40°W. For site 47 this ad-  
520 ditional filter was not necessary, because on the northern Brazilian coastline all of  
521 the swells are due to distant fetches. Therefore, on coastlines exposed to several  
522 kinds of meteorological phenomena, the analysis of  $H_{SP}$  may not be enough to  
523 point to distantly generated swell, and an additional filter would be required.

524 For the second objective, the feasibility of applying the proposed methodology  
525 operationally was illustrated in two cases. Unfortunately wave data near shore  
526 along the Brazilian coast are rarely available, and the criterion used for choosing  
527 these cases was the damage reported by the media. The case of 28 March 2011  
528 corresponds to an extratropical cyclone developing over the South Atlantic; the  
529 waves simulated by WAVEWATCH arrived at site 22 with  $H_S = 2.0$  m, but  $H_S >$   
530 10.0 m in its generating area, about 3700 km away. Although  $H_S$  is small,  $T_p > 15$   
531 s at this site suggested this is a strong event, so further analysis based on the wave

532 power was necessary. Therefore the spectrum was decomposed into several WSs,  
533 and the strongest achieved a maximum of  $H_{SP}^{per} = 1.4$  m, corresponding to a  
534 percentile of 4.7 %.

535 The case of 15 January 2013 represents an extratropical cyclone intensifying  
536 over the North Atlantic: WAVEWATCH simulated  $H_S > 12.0$  m over a distant  
537 region about 6000 km from site 47, which arrived at this site with  $H_S > 3.0$  m and  
538  $T_p > 15$  s. The Hovmöller diagrams for the 5-day forecast of bulk  $H_{SP}^{per}$  showed  
539 percentiles smaller than 1%, but the decomposed spectrum revealed a WS even  
540 stronger, with  $H_{SP}^{per} = 2.9$  m, corresponding to a percentile smaller than 0.1 %.

541 In cases of flooding, the occurrence of storm surge and tide must be consid-  
542 ered, since they can accentuate the effect of the wave attack into the coastline.  
543 A closer inspection showed that in the first case (28 March 2011), the perpen-  
544 dicular wave power alone did not explain the inundation reported at site 22, but  
545 the tide seems to have played a crucial role. In contrast, the inundation reported  
546 in the second case (15 January 2013) was explained just by the percentile of the  
547 perpendicular wave incidence.

548 From this study, one may conclude that the CDT of  $H_{SP}^{per}$  and its percentiles  
549 are useful tools to access the strength of a WS. They can be used as precursors  
550 of floodings along a coastline, but the definition of threshold values will depend  
551 on other properties, that is, even with small  $H_{SP}^{per}$  a flooding can occur when other  
552 effects (e.g. storm surge or tide) are contributing to increasing the water level  
553 near the shore. The determination of the threshold percentile of  $H_{SP}^{per}$  depends  
554 on an extensive knowledge of the region considered, which is possible through

555 observations and simulations on the nearby coast.

556 A possible limitation of this work is the emphasis given to the flux of wave en-  
557 ergy perpendicular to the coast. Since there may be events at some sites where the  
558 parallel propagation is refracted locally towards the coast, resolving these cases  
559 would require more detailed knowledge of the local features of each site.

560 *Acknowledgments.* We thank Dr. Peter Caplan for his comments and sug-  
561 gestions for improving the English version of this manuscript. This research was  
562 supported by Fundação de Amparo à pesquisa do Estado de São Paulo (FAPESP),  
563 grant 2005/59438-9.

## 564 **References**

565 Booij, N., R. C. Ris, and L. H. Holthuijsen, 1999: A third-generation wave model  
566 for coastal regions, Part 1, Model description and validation. *J. Geophys.*  
567 *Res.*, **104**,C4, 7649-7666.

568 Brown, J. M., and J. Wolf, 2009 : Coupled wave and surge modelling for the  
569 eastern Irish Sea and implications for model wind-stress. *Continental Shelf*  
570 *Research*, **29**, 1329-1342.

571 Dean, R. and R. Dalrymple, 2003: Water wave mechanics for engineers and  
572 scientists. Singapore, World Scientific, **2**, 353 pp.

573 Gerling, T. W., 1992: Partitioning sequences and arrays of directional wave spec-  
574 tra into component wave systems. *J. Atmos. Ocean. Techn.*, **9**, 444-458.

575 Gray, W. M., and C. W. Landsea, 1992: African rainfall as a precursor of hurri-  
576 cane -related destruction on the U.S. East Coast. *Bull. Amer. Meteor. Soc.*,  
577 **73**, 1352-1364.

578 Hanson, J. L., and O. M. Phillips, 2001: Automated analysis of ocean surface  
579 directional wave spectra. *J. Atmos. Ocean. Techn.*, **18**, 277-293.

580 Hasselmann, S., K. Hasselmann, C. Bruning, and G. Komen, 1994: Extraction of  
581 wave spectra from SAR image spectra, in dynamics and modeling of ocean  
582 waves. England: Cambridge Univ. Press, Cambridge.

- 583 Innocentini, V., S.C.S.C. Prado, C.S. Pereira, F.O. Arantes, and I. N. Brandao,  
584 2001 : Ocorrencia de vagas no arquipelago de Sao Pedro e Sao Paulo: caso  
585 outubro de 1999 *Revista Brasileira de Meteorologia*, **16**, 177-186.
- 586 Innocentini, V. and E. S. Caetano Neto, 1996: A case study of the 9 August 1988  
587 South Atlantic storm: numerical simulations of the wave activity. *Wea.*  
588 *Forecasting*, **11**, 78-88.
- 589 Kalnay, E., and Coauthors, 1996: NCEP/NCAR 40-Year Reanalysis Project.  
590 *Bull. Amer. Meteor. Soc.*, **77**, 437-471.
- 591 Machado, A. A., L. J. Calliari, E. Melo, and A. H. F. Klein, 2010: Historical as-  
592 sessment of extreme coastal sea state conditions in southern Brazil and their  
593 relation to erosion episodes. *Pan-American Journal of Aquatic Sciences*, **5**,  
594 277-286.
- 595 Paice, N., 1998: Autumnal funnel clouds over west Hampshire: A precursor to  
596 wintertime tornadoes. *Weather*, **53**, 419-424.
- 597 Portilla, J., F. J. Ocampo-Torres, and J. Monbaliu, 2009: Spectral partitioning  
598 and identification of wind sea and swell. *J. Atmos. Oceanic Technol.*, **26**,  
599 107-122.
- 600 Rocha, R. P., S. Sugahara, and V. Innocentini, 2000: Marine cyclones over South  
601 Atlantic Ocean during 1999 winter. Part I: Their structure, intensity and  
602 evolution. *Preprints, Sixth Int. Conf. on Southern Hemisphere Meteorology*  
603 *and Oceanography*, Santiago, Chile, Amer. Meteor. Soc., 200-201.

- 604 Rocha, R. P., S. Sugahara, and R. B. Silveira, 2004: Sea waves generated by  
605 extratropical cyclones in the South Atlantic Ocean: Hindcast and validation  
606 against altimeter data. *Wea. Forecasting* **19**, 398-410.
- 607 Saha, and Coauthors, 2010: The NCEP Climate Forecast System Reanalysis.  
608 *Bull. Amer. Meteor. Soc.*, **91**, 1017-1058.
- 609 Sasaki, W., 2012: Changes in wave energy resources around Japan. *Geophysical*  
610 *Research Letters*, **39**, n/a-n/a.
- 611 Sinclair, M.R., 1995: A climatology of cyclogenesis for the Southern Hemi-  
612 sphere. *Mon. Wea. Rev.*, **123**, 1601-1619.
- 613 Tolman, H.L., 2008: User manual and system documentation os WAVEWATCH  
614 III version 3.14. NOAA/NWS/NCEP/MMAB Technical note **278**, 194 pp.
- 615 Young, I.R., 1999: Wind Generated Ocean Waves, Volume 2, Elsevier Ocean  
616 Engineering Book Series, 288 pp.



## 617 **List of Figures**

618 FIG. 1. The 3 domains nested into the global domain used by the WAVEWATCH  
619 simulations to build the 31-year database, and the location of 61 monitoring sites,  
620 lying nearly on the 100-m isobath following the Brazilian coastline. Areas shall-  
621 lower than 1000 m are represented by gray. The spatial resolution is  $0.625^\circ \times$   
622  $0.625^\circ$  and  $0.3125^\circ \times 0.3125^\circ$  for the global and nested domains, respectively.

623

624 FIG. 2. The percentile (contour in %) of the 61 sites for the component of the  
625 potential significant height perpendicular to the 100-m isobath at each site ( $H_{SP}^{per}$ ),  
626 computed from the 31-year database.

627

628 FIG. 3. Significant wave height ( $H_S$ ), potential significant wave height ( $H_{SP}$ ),  
629 and its component perpendicular to the coast ( $H_{SP}^{per}$ ), for the 50 highest  $H_{SP}^{per}$  sim-  
630 ulated for sites (a) 22 and (b) 47. The units are meters.

631

632 FIG. 4. Trajectories of the cyclones responsible for the 15 events listed at Table 1,  
633 occurring in the South Atlantic. The central position of the area with maximum  
634 surface speed, if greater than  $20 \text{ m s}^{-1}$ , is used to track each trajectory.

635

636 FIG. 5. As in Fig. 4, but for the 10 first events listed in Table 2, occurring in the  
637 North Atlantic.

638

639 FIG. 6. Contours of surface wind speed  $U_{10}$  ( $\text{m s}^{-1}$ ) and streamlines at 2100 UTC  
640 28 March 2011.

641

642 FIG. 7. Significant wave height  $H_S$  (m) and mean wave direction at 0600 UTC 29  
643 April 2011.

644

645 FIG. 8. Time evolution of significant wave height  $H_S$  (m), wind speed  $U_{10}$  ( $\text{m s}^{-1}$ )  
646 ), and peak period  $T_p$  (s) at site 22, from 30 March to 03 April 2011.

647

648 FIG. 9. Spectrum for the site 22 at 1800 UTC 01 April 2011. The units are  $\text{m}^2\text{s}$   
649  $\text{rad}^{-1}$ . The plotting interval is 0.1, 1, and 10 for contours smaller than 1, 10 and  
650 100, respectively. The circle represents the period (s). The convention for propa-  
651 gation direction is from the center towards the plotted contour.

652

653 FIG. 10. Hovmöller diagram for the 61 sites of the perpendicular component of  
654 the potential significant height  $H_{SP}^{per}$  (m), from 28 March to 03 April 2011, in (a)  
655 meters and (b) percentile (%). The vertical dashed line delimits the forecast pe-  
656 riod, starting at 00 UTC 30 March 2011.

657

658 FIG. 11. Time evolution of the perpendicular component of the potential signif-  
659 icant height  $H_{SP}^{per}$  (m) for individual wave systems (WS), from 30 March to 02  
660 April 2011. The horizontal dashed line indicates the percentile of the strongest  
661  $H_{SP}^{per}$  during the 4-day period.

662

663 FIG. 12. Wind field  $U_{10}$ , as in Fig. 6, but at 1800 UTC 11 January 2013.

664

665 FIG. 13. Significant wave height  $H_S$ , as in Fig. 7, but at 0900 UTC 12 January  
666 2013.

667

668 FIG. 14. Time evolution as in Fig. 8, but at site 47, from 13 to 17 January 2013.

669

670 FIG. 15. Spectrum as in Fig. 9, but for the site 47 at 0600 UTC 16 January 2013.

671

672 FIG. 16. Hovmöller diagram for  $H_{SP}^{per}$  and its percentile, as in Fig. 10, but from  
673 12 to 18 January 2013. Forecast starting at 00 UTC 14 January 2013.

674

675 FIG. 17. Time evolution of  $H_{SP}^{per}$  for the wave systems, like Fig. 11, but at site 47  
676 from 13 to 16 January 2013.

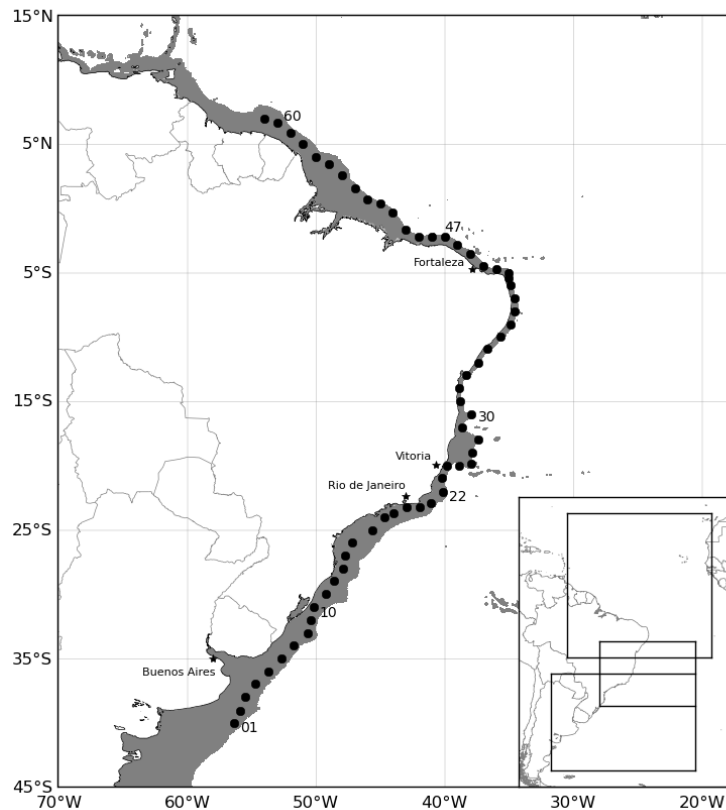
677

678 **List of tables**

679 TABLE 1. Cases with significant wave height  $H_S \leq 1.8$  m selected from the  
680 50 cases for the site 22 presented in Fig.3a. The first column refers to the event  
681 number presented in the figure. The properties shown are significant wave height  
682 ( $H_S$ ), potential significant wave height ( $H_{SP}$ ), and its component perpendicular  
683 to the coast ( $H_{SP}^{per}$ ).

684 TABLE 2. Main properties, as in Table 1, but for the first 10 cases presented at  
685 Fig.3b.

686 **Figures**

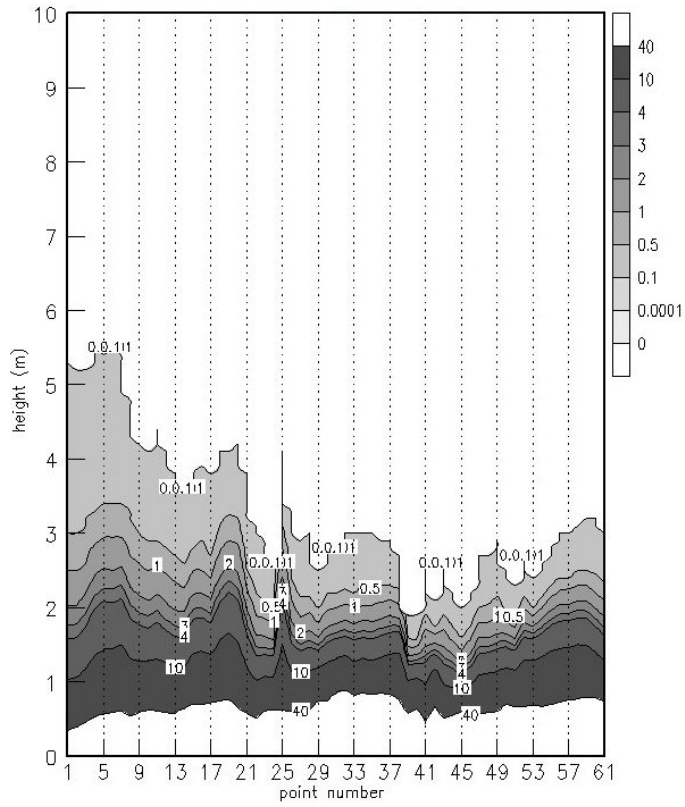


687

688

689 FIG. 1. The 3 domains nested into the global domain used by the WAVEWATCH  
690 simulations to build the 31-year database, and the location of 61 monitoring sites,  
691 lying nearly on the 100-m isobath following the Brazilian coastline. Areas shall-  
692 lower than 1000 m are represented by gray. The spatial resolution is  $0.625^\circ \times$   
693  $0.625^\circ$  and  $0.3125^\circ \times 0.3125^\circ$  for the global and nested domains, respectively.

694

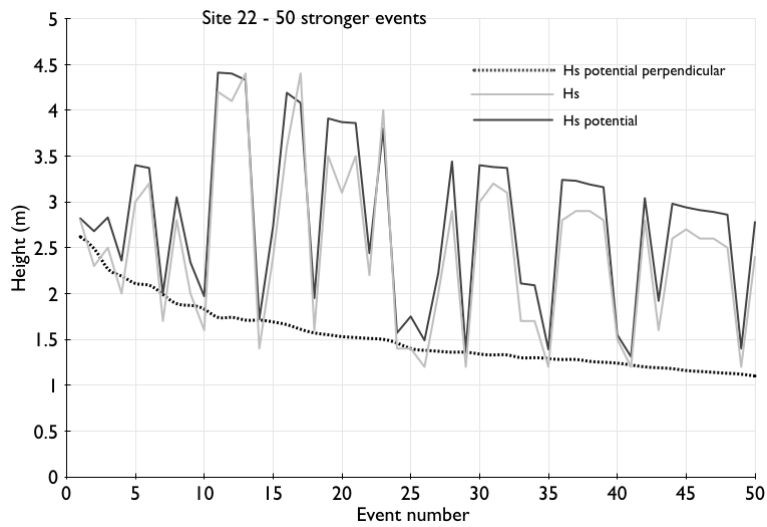


695

696

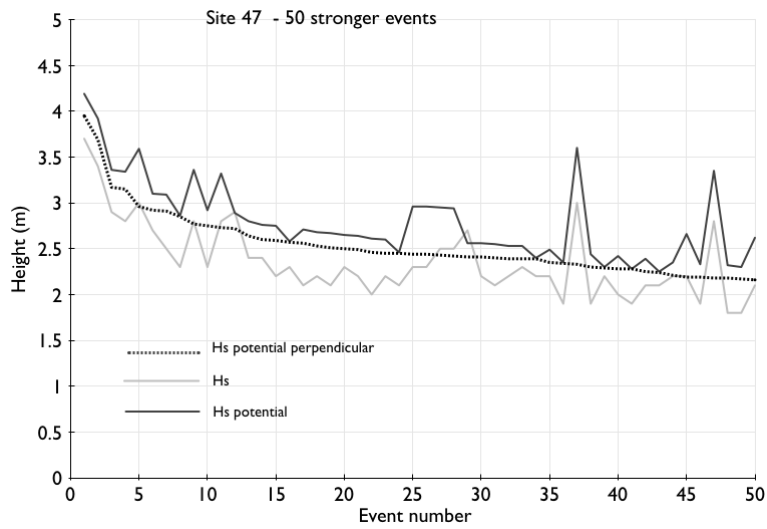
697 FIG. 2. The percentile (contour in %) of the 61 sites for the component of the  
 698 potential significant height perpendicular to the 100-m isobath at each site ( $H_{SP}^{per}$ ),  
 699 computed from the 31-year database.

700



701 FIG. 3a

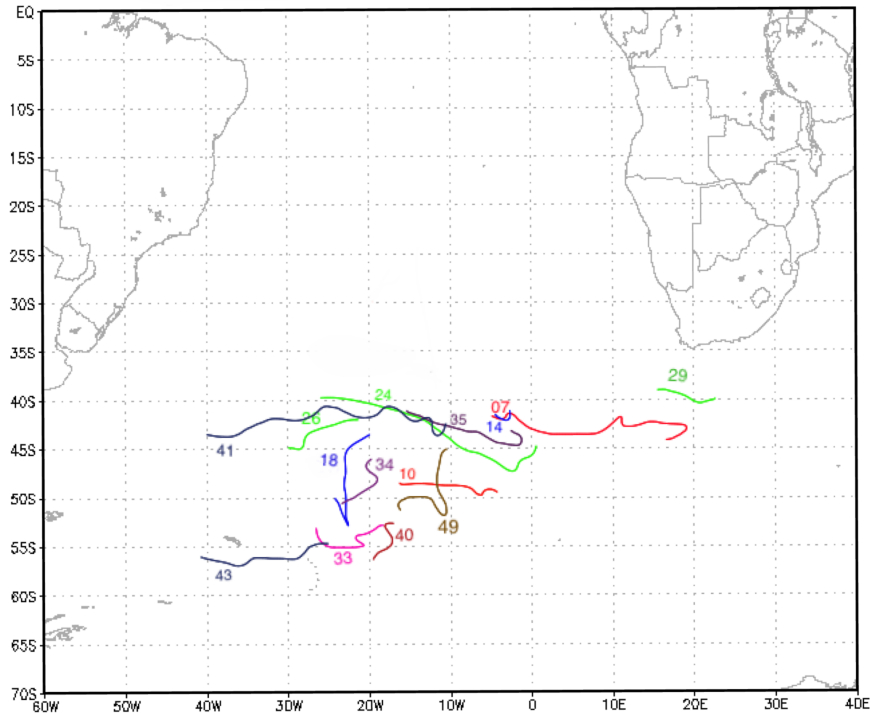
702



703 FIG. 3b

704

705 FIG. 3. Significant wave height ( $H_S$ ), potential significant wave height ( $H_{SP}$ ), and  
 706 its component perpendicular to the coast ( $H_{SP}^{per}$ ), for the 50 highest  $H_{SP}^{per}$  simulated  
 707 for sites (a) 22 and (b) 47. The units are meters.



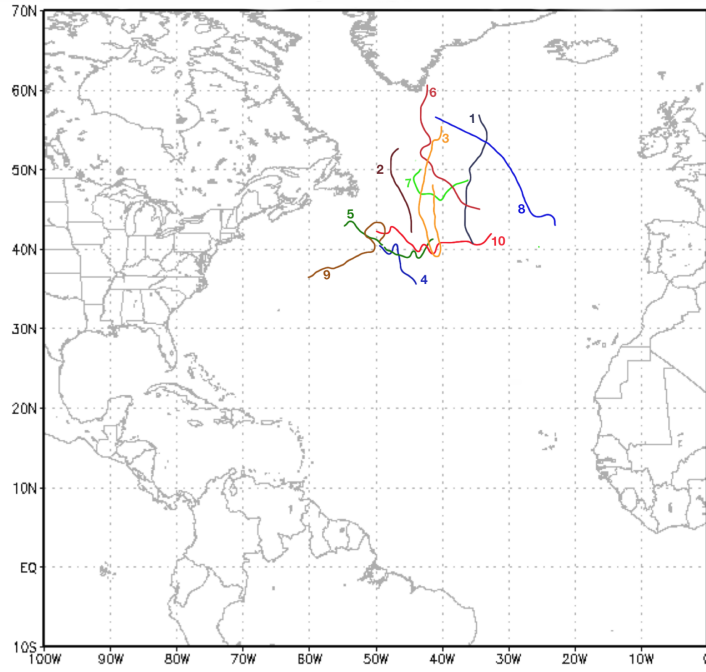
708

709

710 FIG. 4. Trajectories of the cyclones responsible for the 15 events listed at Table 1,  
 711 occurring in the South Atlantic. The central position of the area with maximum  
 712 surface speed, if greater than  $20 \text{ m s}^{-1}$ , is used to track each trajectory.

713



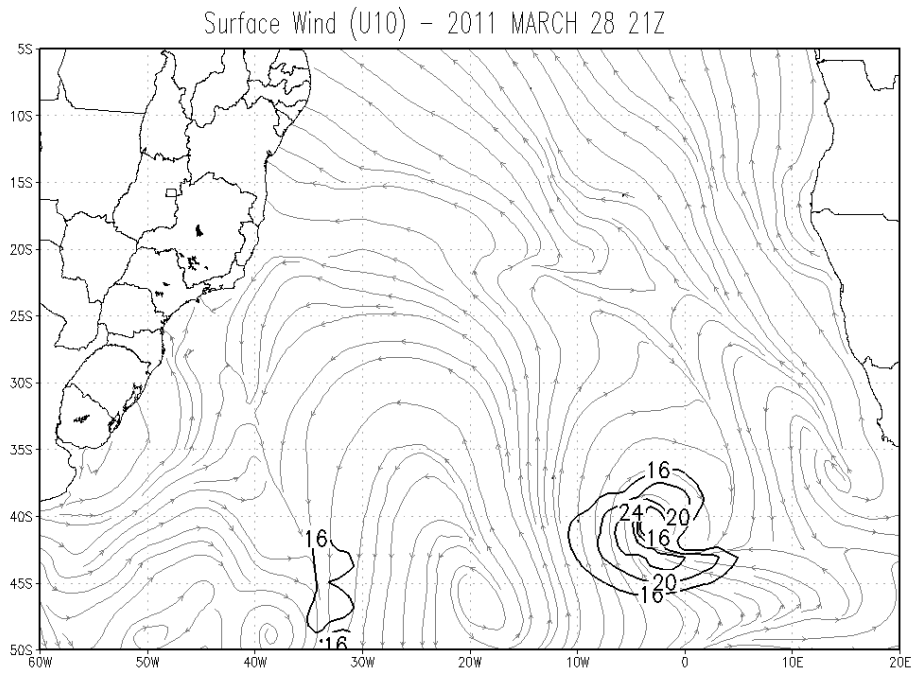


714

715

716 FIG. 5. As in Fig. 4, but for the 10 first events listed in Table 2, occurring in the  
717 North Atlantic.

718



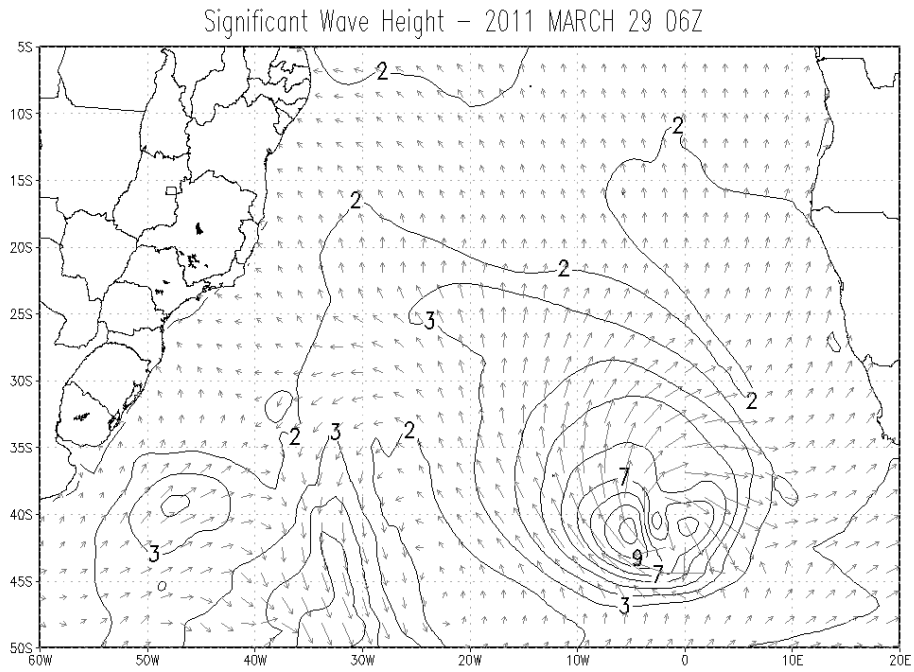
719

720

721 FIG. 6. Contours of surface wind speed  $U_{10}$  ( $\text{m s}^{-1}$ ) and streamlines at 2100 UTC

722 28 March 2011.

723

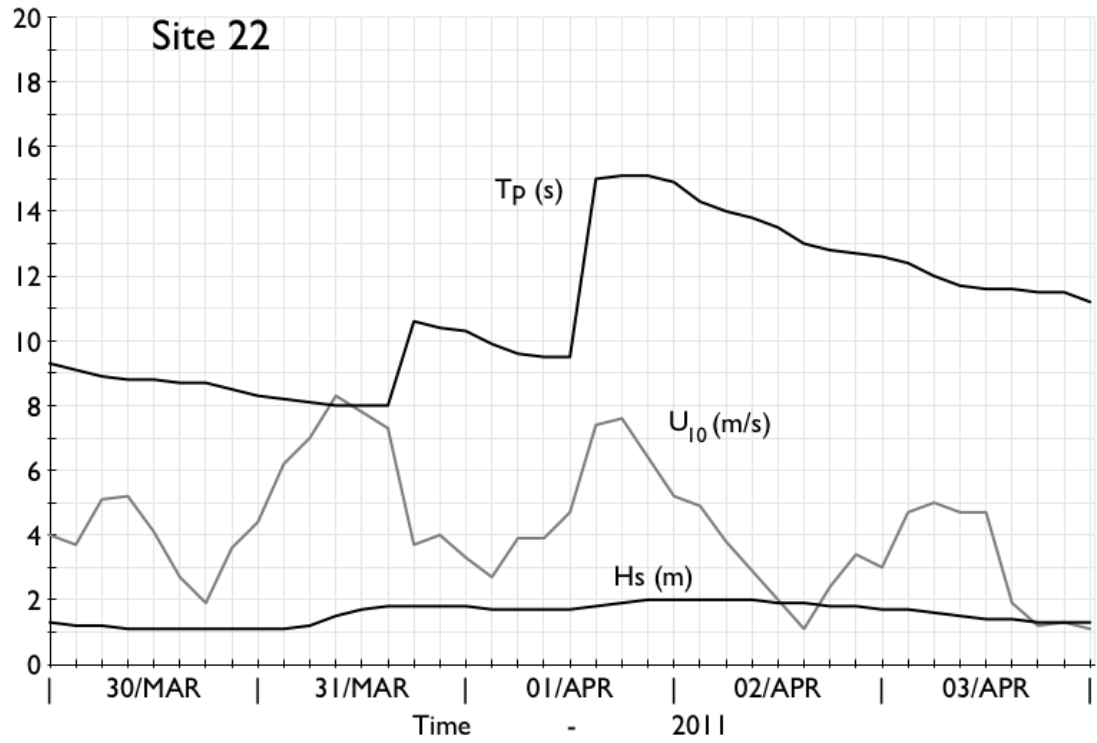


724

725

726 FIG. 7. Significant wave height  $H_S$  (m) and mean wave direction at 0600 UTC 29  
 727 April 2011.

728

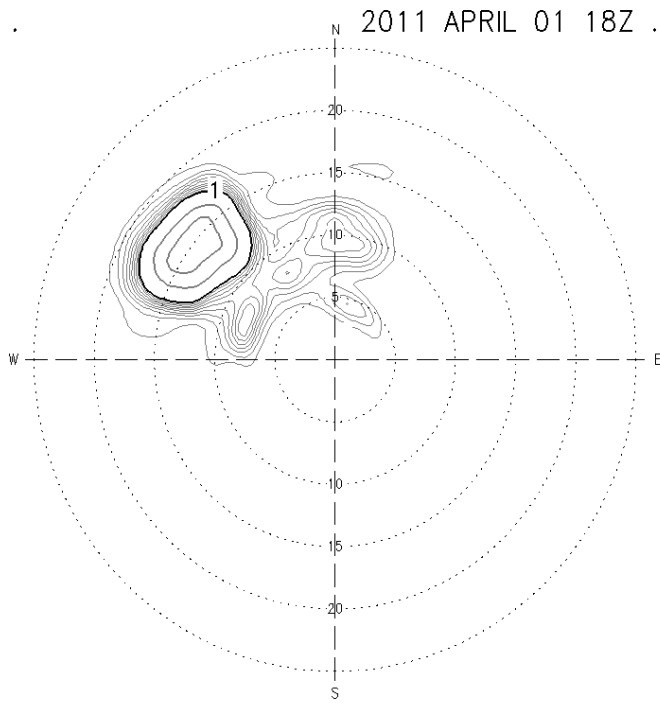


729

730

731 FIG. 8. Time evolution of significant wave height  $H_S$  (m), wind speed  $U_{10}$  ( $\text{m s}^{-1}$ )  
 732 ), and peak period  $T_p$  (s) at site 22, from 30 March to 03 April 2011.

733

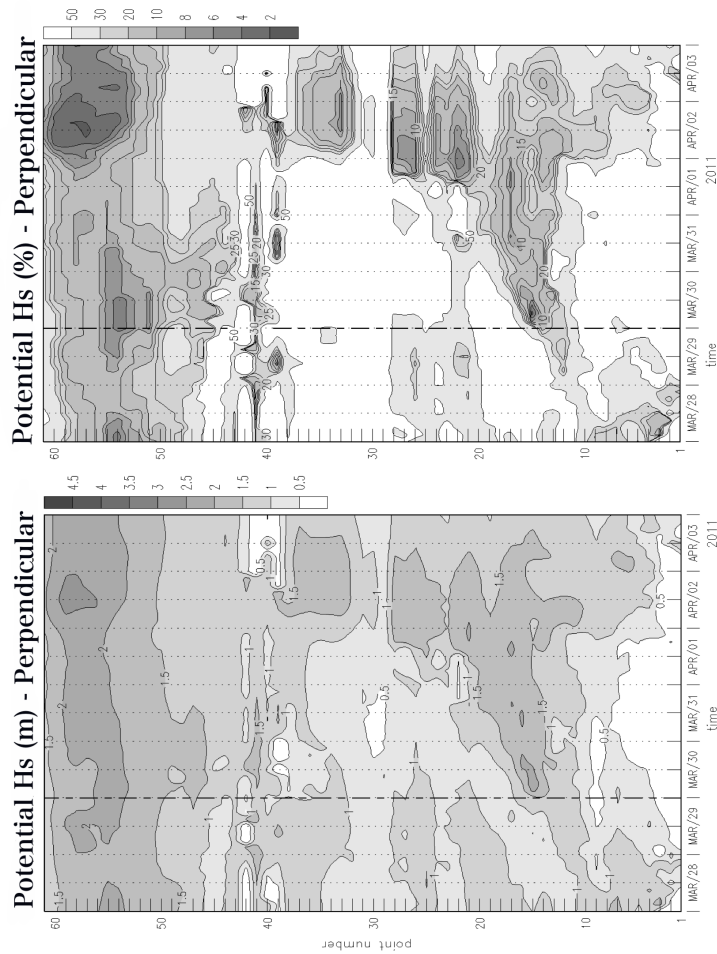


734

735

736 FIG. 9. Spectrum for the site 22 at 1800 UTC 01 April 2011. The units are  $\text{m}^2\text{s}$   
 737  $\text{rad}^{-1}$ . The plotting interval is 0.1, 1, and 10 for contours smaller than 1, 10 and  
 738 100, respectively. The circle represents the period (s). The convention for propa-  
 739 gation direction is from the center towards the plotted contour.

740

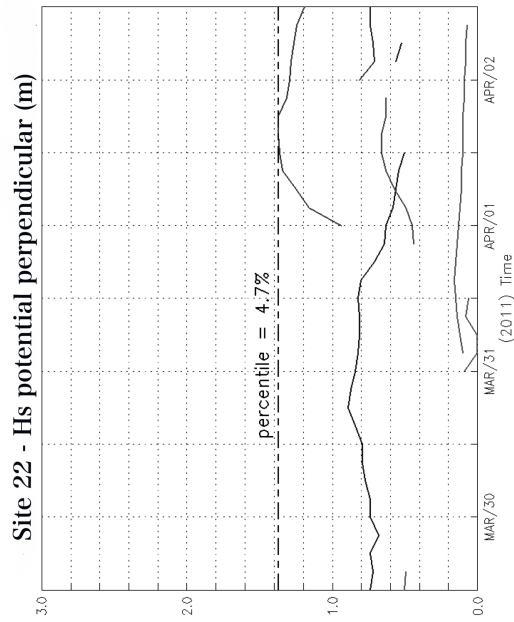


741

742

743 FIG. 10. Hovmöller diagram for the 61 sites of the perpendicular component of  
 744 the potential significant height  $H_{SP}^{per}$  (m), from 28 March to 03 April 2011, in (a)  
 745 meters and (b) percentile (%). The vertical dashed line delimits the forecast pe-  
 746 riod, starting at 00 UTC 30 March 2011.

747

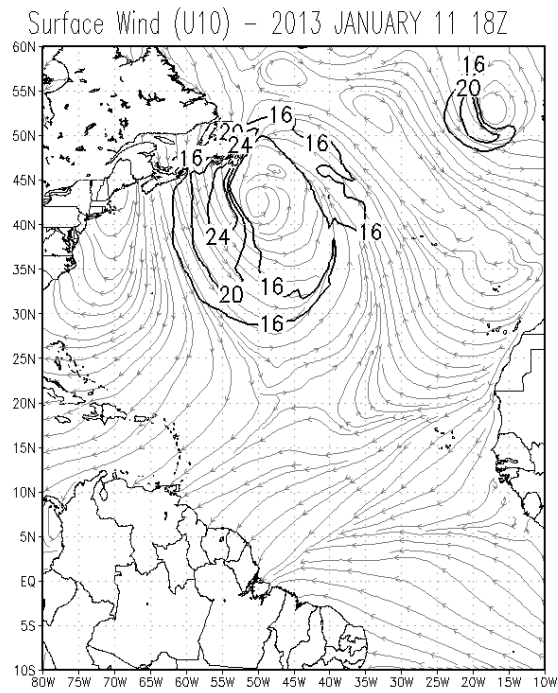


748

749

750 FIG. 11. Time evolution of the perpendicular component of the potential signif-  
 751 icant height  $H_{SP}^{per}$  (m) for individual wave systems (WS), from 30 March to 02  
 752 April 2011. The horizontal dashed line indicates the percentile of the strongest  
 753  $H_{SP}^{per}$  during the 4-day period.

754



755

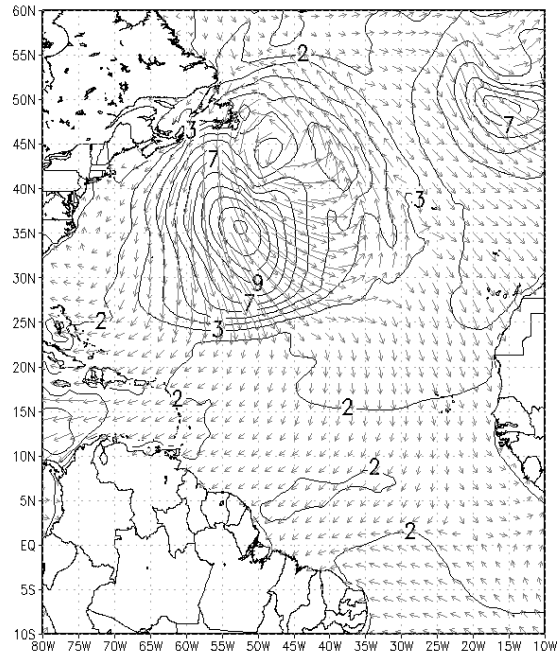
756

757 FIG. 12. Wind field  $U_{10}$ , as in Fig. 6, but at 1800 UTC 11 January 2013.

758



Significant Wave Height – 2013 JANUARY 12 09Z

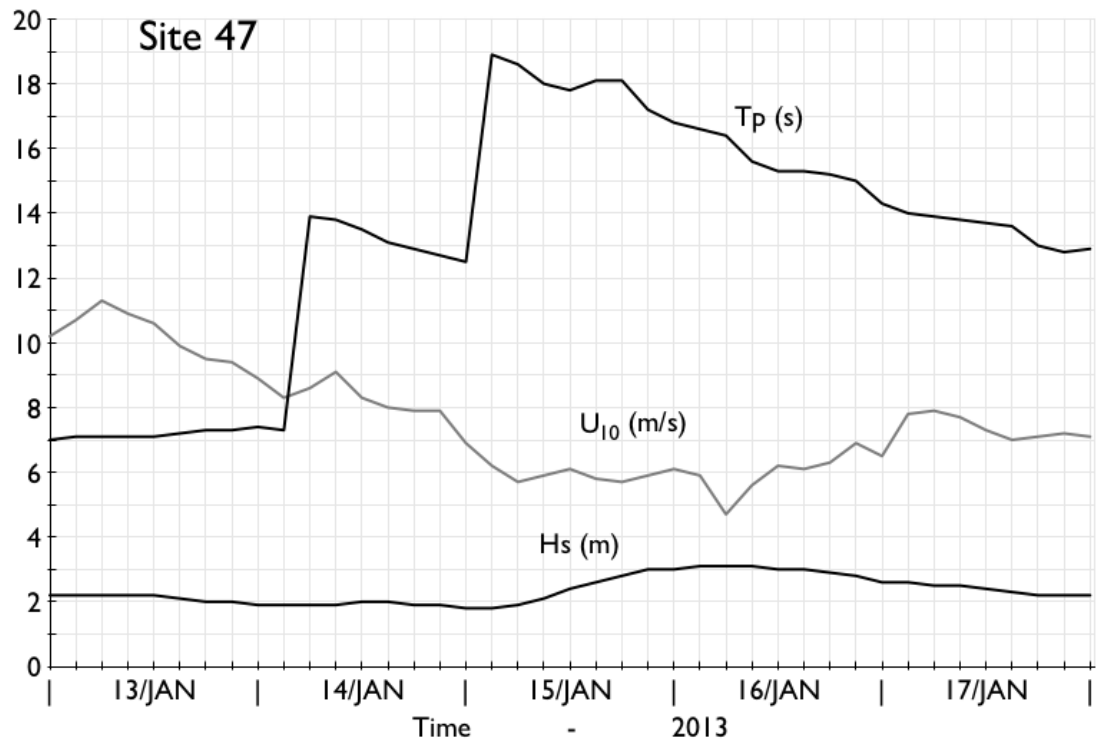


759

760

761 FIG. 13. Significant wave height  $H_S$ , as in Fig. 7, but at 0900 UTC 12 January  
762 2013.

763

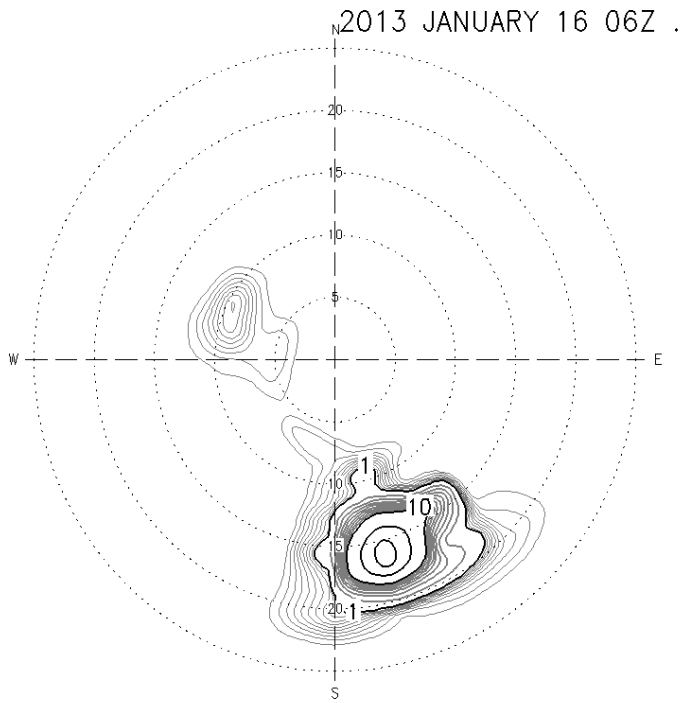


764

765

766 FIG. 14. Time evolution as in Fig. 8, but at site 47, from 13 to 17 January 2013.

767

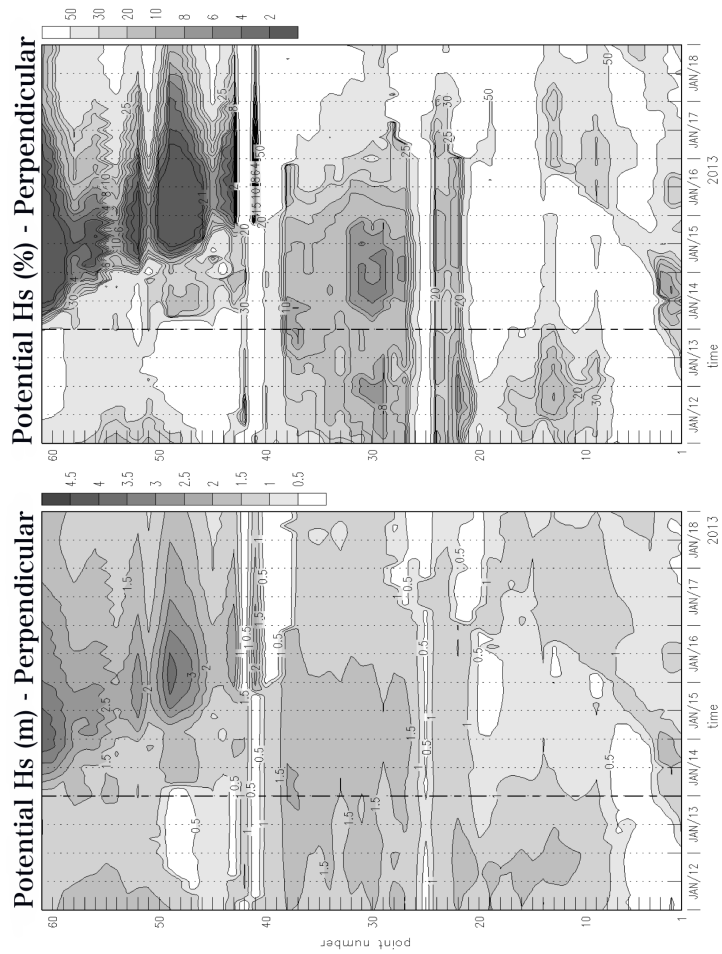


768

769

770 FIG. 15. Spectrum as in Fig. 9, but for the site 47 at 0600 UTC 16 January 2013.

771

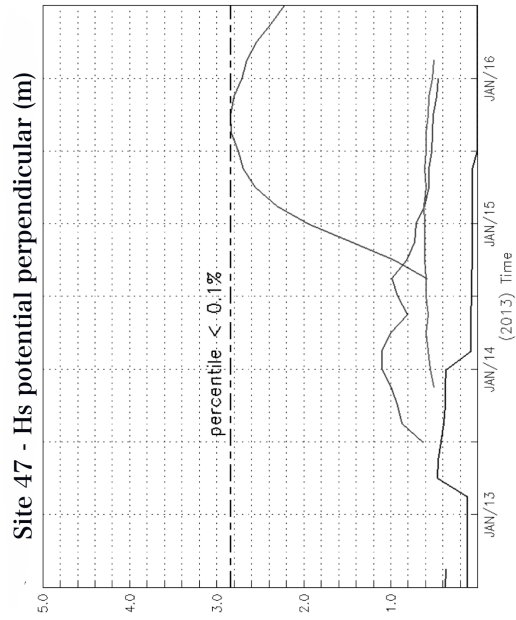


772

773

774 FIG. 16. Hovmöller diagram for  $H_{SP}^{per}$  and its percentile, as in Fig. 10, but from  
 775 12 to 18 January 2013. Forecast starting at 00 UTC 14 January 2013.

776



777

778

779 FIG. 17. Time evolution of  $H_{SP}^{per}$  for the wave systems, like Fig. 11, but at site 47  
 780 from 13 to 16 January 2013.

781

782 **Tables**

event	date	$H_S$	$H_{SP}$	$H_{SP}^{per}$
7	1986 06 02	1.7	2.00	1.99
10	1990 08 13	1.6	1.97	1.83
14	1986 05 31	1.4	1.72	1.71
18	1998 05 18	1.6	1.95	1.57
24	1979 08 01	1.4	1.57	1.46
25	1980 03 17	1.4	1.75	1.40
26	1979 08 08	1.2	1.49	1.38
29	2007 06 10	1.2	1.37	1.36
33	1983 09 16	1.7	2.11	1.30
34	1996 08 23	1.7	2.09	1.30
35	2004 10 18	1.2	1.39	1.29
40	1982 06 09	1.5	1.55	1.24
41	1984 07 12	1.2	1.31	1.22
43	2003 05 25	1.6	1.92	1.19
49	1992 03 07	1.2	1.40	1.12

783 TABLE 1. Cases with significant wave height  $H_S \leq 1.8$  m selected from the  
784 50 cases for the site 22 presented in Fig.3a. The first column refers to the event  
785 number presented in the figure. The properties shown are significant wave height  
786 ( $H_S$ ), potential significant wave height ( $H_{SP}$ ), and its component perpendicular  
787 to the coast ( $H_{SP}^{per}$ ).

event	date	$H_S$	$H_{SP}$	$H_{SP}^{per}$
1	1982 02 08	3.7	4.19	3.95
2	1983 12 27	3.4	3.92	3.69
3	1985 12 07	2.9	3.36	3.17
4	2009 12 31	2.8	3.34	3.15
5	1982 01 05	3.0	3.59	2.96
6	1996 12 24	2.7	3.10	2.92
7	2005 10 18	2.5	3.09	2.91
8	1989 11 23	2.3	2.86	2.85
9	2010 02 10	2.8	3.36	2.77
10	1985 02 09	2.3	2.92	2.75

788 TABLE 2. Main properties, as in Table 1, but for the first 10 cases presented at  
789 Fig.3b.